⋈USCAP

ARTICLE

Diverse immune environments in human lung tuberculosis granulomas assessed by quantitative multiplexed immunofluorescence

Marta Abengozar-Muela[1] · María Villalba Esparza[1,2,3] · David Garcia-Ros[1,2,4] · Cindy Estefanía Vásquez[4] ·
José I. Echeveste[1,2] · Miguel Angel Idoate[1,2] · Maria D. Lozano[1,2,3] · Ignacio Melero[2,3,5,6] · Carlos E. de Andrea[1,2,3,4]

Abstract

The precise nature of the local immune responses in lung tuberculosis (TB) granulomas requires a comprehensive understanding of their environmental complexities. At its most basic level, a granuloma is a compact, organized immune aggregate of macrophages surrounded by myeloid, B and T cells. We established two complementary multiplex immunolabeling panels to simultaneously evaluate the myeloid and lymphocytic contexture of 14 human lung TB granulomas in formalin-fixed paraffin-embedded tissue samples. We observed diverse CD3+ and CD8+ T-cell and CD20+ B lymphocyte compositions of the granuloma immune environment and a relatively homogeneous distribution of all myeloid cells. We also found significant associations between CD8+ T-cell densities and the myeloid marker CD11b and phagocytic cell marker CD68. In addition, significantly more CD68+ macrophages and CD8+ T cells were found in *Mycobacterium tuberculosis*-infected granulomas, as detected by Ziehl–Neelsen staining. FOXP3 expression was predominately found in a small subset of CD4+ T cells in different granulomas. As the success or failure of each granuloma is determined by the immune response within that granuloma at a local and not a systemic level, we attempted to identify the presence of reactive T cells based on expression of the T-cell activation marker CD137 (4-1BB) and programmed cell death-1 (PD-1). Only a small fraction of the CD4+ and CD8+ T cells expressed PD-1. CD137 expression was found only in a very small fraction of the CD4+ T cells in two granulomas. Our results also showed that multinucleated giant cells showed strong PD-L1 but not CTLA-4 membrane staining. This study offers new insights into the heterogeneity of immune cell infiltration in lung TB granulomas, suggesting that each TB granuloma represents a unique immune environment that might be independently influenced by the local adaptive immune response, bacterial state, and overall host disease status.

These authors contributed equally: Ignacio Melero, Carlos E. de Andrea

Supplementary information The online version of this article (https://doi.org/10.1038/s41379-020-0600-6) contains supplementary material, which is available to authorized users.

✉ Carlos E. de Andrea
ceandrea@unav.es

1 Department of Pathology, Clínica Universidad de Navarra, University of Navarra, Pamplona, Spain

2 Navarra Institute for Health Research (IDISNA), Pamplona, Spain

3 Centro de Investigación Biomédica en Red de Cáncer (CIBERONC), Madrid, Spain

4 Department of Anatomy, Physiology and Pathology, University of Navarra, Pamplona, Spain

5 Department of Immunology and Immunotherapy, Clínica Universidad de Navarra, Pamplona, Spain

6 Program of Immunology and Immunotherapy, Cima Universidad de Navarra, Pamplona, Spain

Introduction

Tuberculosis (TB) is an infectious disease caused by microorganisms of the *Mycobacterium tuberculosis* complex (Mtb) [1, 2]. According to the World Health Organization, in 2018, an estimated ten million people developed active TB disease, of whom 1.2 million died [1, 3]. Clinically, TB can be presented as a spectrum from asymptomatic infection to life-threatening disease [2]. Histologically, TB is the most common cause of infectious granuloma worldwide.

The formation and maintenance of TB granulomas are complex and immunologically dynamic. Granulomas are organized immune cell aggregates that originate in response to persistent stimuli of an infectious or

noninfectious nature. TB granulomas are not only involved in the control of Mtb infection but also, in some cases, in its persistence. From the host perspective, granulomas are a bacterial "prison" with the potential to isolate the infection from the rest of the body; however, from the bacterial perspective, they represent a growing collection of macrophages than can be infected and provide a haven for replication [1]. This dual role of the TB granuloma conceivably gives rise to distinct inflammatory immune environments.

Infection begins when Mtb enters the lungs through inhalation and reaches the alveolar space. If the resident alveolar macrophages fail to eliminate the bacteria, Mtb invades the lung interstitial tissue either by directly infecting the alveolar epithelium or the alveolar macrophages [4]. Dendritic cells and inflammatory monocytes can then transport Mtb to pulmonary lymph nodes for T-cell priming. This event is believed to be critical to initiate granuloma formation by recruiting immune cells, including CD4+ and CD8+ T cells and CD20+ B lymphocytes, to the lung parenchyma [1].

Macrophages play an essential role in TB granuloma formation [5]. They both harbor Mtb and possess effector functions to kill Mtb. The host response to Mtb infection triggers the differentiation of granuloma macrophages into epithelioid macrophages and multinucleated giant cells (MGCs) that are unable to mediate any bacterial uptake [6]. The immune cell activation occurring at the granuloma site may initiate the classical central necrosis that may undergo caseation and liquefaction.

The formation and maintenance of TB granulomas are orchestrated by tumor necrosis factor (TNF), interferon-γ, interleukin-12, and other signaling molecules that mediate monocyte and macrophage migration [2]. TNF also has additional effects on the structure of the granuloma in the context of adaptive immunity by influencing processes such as T-cell trafficking and activation [2].

The TB paradox is that despite the concentration of vigorous host immune responses in granulomas, reinfection and bacterial persistence frequently occur [2, 7]. Host responses rarely result in complete eradication and clearance of Mtb, but rather limit the infection to a dormant state [8, 9]. The granuloma structure may also contribute to disease progression and host outcome by limiting macrophage interactions with other immune cells.

Exploration of the immune environment of lung TB granulomas would offer insights into their complex and heterogeneous composition. Thus, we sought to investigate the myeloid and lymphocytic contexture of human lung TB granulomas in formalin-fixed paraffin-embedded (FFPE) tissue samples. A novel tyramide signal amplification (TSA) multiplexing technique was used to enable the simultaneous examination of six cellular markers. Two seven-color multiplex panels were developed and validated targeting the myeloid marker CD11b, the phagocytic cell marker CD68 of macrophages, CD3+, CD4+, and CD8+ T cells, and CD20+ B lymphocytes. Additional markers included the transcription factor FOXP3, the bona fide T-cell activation marker CD137 (4-1BB), programmed cell death-1 (PD-1), and cytokeratin. We also evaluated the protein expression of the immune checkpoint molecules programmed cell death ligand-1 (PD-L1) and cytotoxic T-lymphocyte-associated protein 4 (CTLA-4). Our results revealed distinct lymphoid and myeloid cell subpopulations populate TB granulomas with specific spatial distributions and associations. Significantly more cells expressing the phagocytic cell marker CD68 of macrophages and CD8+ T cells were found in Mtb-infected granulomas, as detected by Ziehl–Neelsen staining and light microscopy. We also observed that granuloma macrophages and MGCs were positive for PD-L1 but not CTLA-4.

Materials and methods

Histology

Whole tissue sections were obtained from 14 human lung TB granulomas (Supplementary Table 1 for details). Sample selection was based on histological evidence of TB and PCR positivity for Mtb DNA. All TB granulomas samples were collected from HIV-negative patients. FFPE tissue samples were obtained with informed patients' consent and retrieved from the pathology files of the Clínica Universidad de Navarra (protocol 111/2010). Histological evidence of TB granulomas with central necrosis surrounded by a highly cellular area at the periphery were evaluated based on the review of hematoxylin and eosin-stained sections from FFPE blocks by two authors of this study (CEA and MAM). In addition, the detection of acid-fast bacilli (AFB) was investigated in all cases by the conventional Ziehl–Neelsen method, as described elsewhere [10]. The presence of Mtb DNA in tissue samples was performed as part of the routine diagnostic guidelines of the Clínica Universidad de Navarra by using a commercially available multiplex PCR-based, solid-phase reverse hybridization GenoType MTBC assay (Hain Lifescience GmbH, Nehren, Germany) [11].

Multiplex immunofluorescence staining

Four-micron sections from FFPE tissue samples of human lung TB granulomas and control tonsil tissue were used for (1) the initial setup of staining conditions for each single
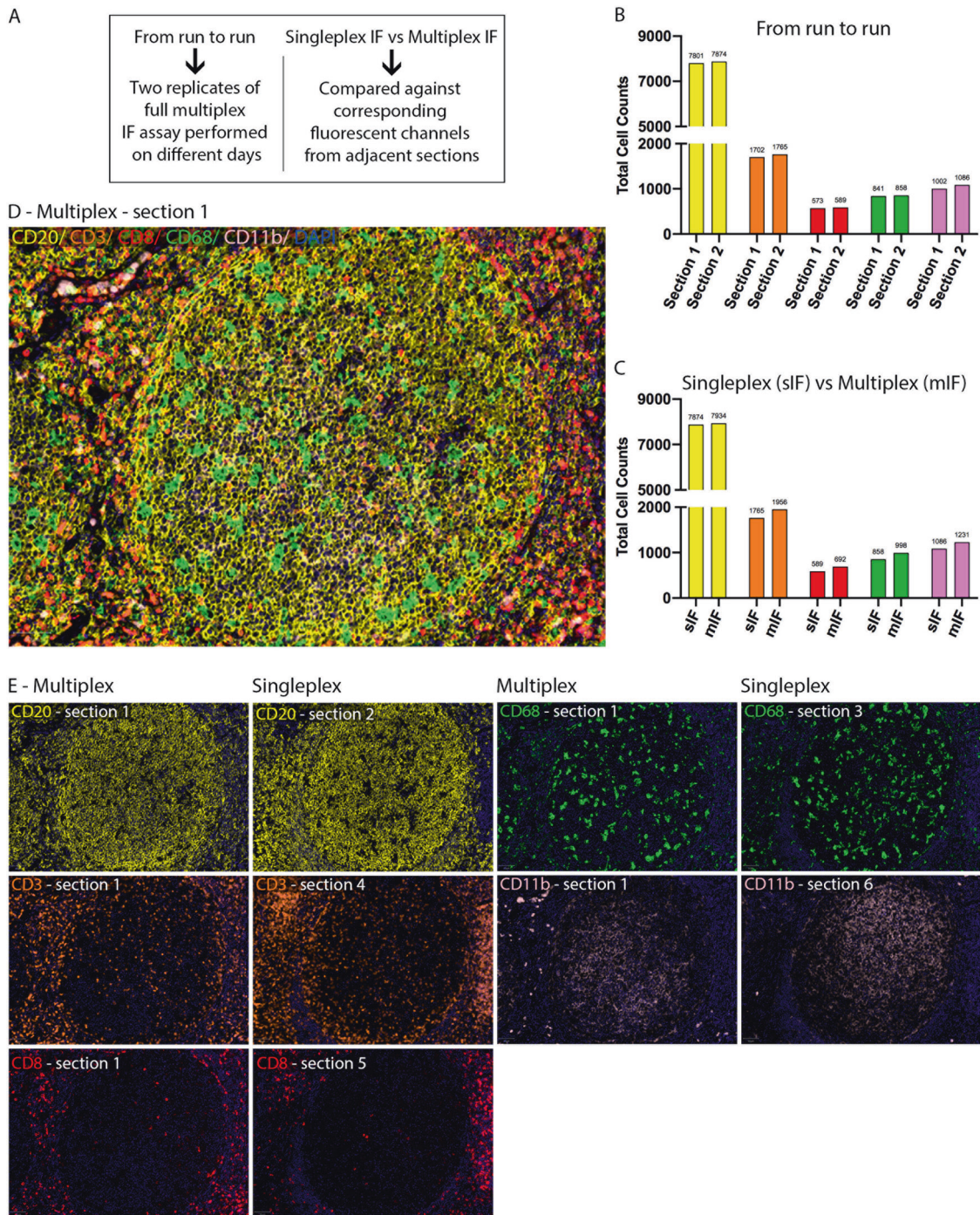
Fig. 1 Seven-color multiplex staining protocols. a Validation workflow. **b** Total number of cells for each marker, comparing replicates of the full multiplex immunofluorescence (mIF) protocol on sequential FFPE tonsil sections (sections 1 and 2) performed on different days. **c** Total number of cells for each marker, comparing the singleplex IF against corresponding fluorescent channel from mIF on sequential FFPE tonsil sections. **d** Spectrally unmixed composite image of FFPE human tonsil section stained for CD11b (clone EPR1344, Opal, pink), CD68 (clone PG-M1, Opal, green), CD3 (IgG, Opal, orange), CD8 (clone C8/144B, Opal, red), CD20 (clone L26, Opal, yellow), cytokeratin (clone AE1/AE3, Opal, cyan, not shown in the images), and DAPI (Dark Blue). **e** Multiplex IF images were compared against the corresponding fluorescent channel from singleplex IF images from sequential tissue sections (mIF on section 1; sIF on sections 2–6). Scale bars represent 50 μm.

primary antibody and (2) the successive optimization of the Opal seven-color multiplex immunolabeling protocols.

In the first step, primary antibodies against the antigens listed below were established as single stains initially in human tonsil tissue and thereafter on lung TB granulomas.

The multiplex assay development and validation is summarized in Fig. 1a–e and Supplementary Fig. 1.

The myeloid and lymphoid cell panel included CD11b (rabbit monoclonal, clone EPR1344, 1:1000, Abcam, product number ab133357), CD68 (mouse monoclonal, clone PG-M1, ready-to-use, Agilent, product number IR613), CD3 (rabbit polyclonal, IgG, ready-to-use, Agilent, product number IR503), CD8 (mouse monoclonal, clone C8/144B, ready-to-use, Agilent, product number GA62361-2), CD20 (mouse monoclonal, IgG2α, clone L26, ready-to-use, Agilent, product number GA604), and cytokeratin (mouse monoclonal, clone AE1/AE3, ready-to-use, Leica Biosystems, product number NCL-L-AE1/AE).

The reactive T-cell panel included CD4 (mouse monoclonal, clone 4B12, ready-to-use, Agilent, product number IS64930-2), CD8 (mouse monoclonal, clone C8/144B, ready-to-use, Agilent, product number GA62361-2), FOXP3 (mouse monoclonal, clone 236A/E7, 1:300, Abcam, product number ab20034), PD-1 (mouse monoclonal, clone NAT105, ready-to-use, Cell Marque, product number 315M), CD137 (TNFRSF9 or 4-1BB, mouse monoclonal, clone BBK-2, 1:80, ThermoFisher, product number MA5-13736), and cytokeratin (mouse monoclonal, clone AE1/AE3, ready-to-use, Leica Biosystems, product number NCL-L-AE1/AE).

In a second step, opal seven-color multiplex immunofluorescence protocols were developed essentially as described previously [12–15]. Each section was exposed to seven sequential rounds of antibody staining. These sequential rounds may lead to random binding of antibodies, imbalanced signals, incomplete staining through interference with previously applied TSA, disruption of epitopes, and removal of TSA fluorophores due to repetitive antigen retrievals at high temperature [13, 14, 16]. Therefore, each single antibody was optimized individually for its optimal conditions and position in the sequence of multiplex staining to reduce interference with previous antibody–TSA complexes or by disruption of epitopes (Fig. 1a–e and Supplementary Fig. 1).

For multiplex immunofluorescence staining, 4-μm sections obtained from FFPE blocks were deparaffinized and the tissues fixed with formaldehyde:methanol (1:10) prior to antigen retrieval. Antigen retrieval was performed using DAKO PT-Link heat induced antigen retrieval with low pH (pH 6) or high pH (pH 9) target retrieval solution (Dako, Glostrup, Denmark). Each section was subjected to six successive rounds of antibody staining, each consisting of protein blocking with 20% normal goat serum (Dako) in phosphate-buffered saline, incubation with primary antibody, biotinylated anti-mouse/rabbit secondary antibodies, and Streptavidin-HRP (Dako, 50003), followed by TSA visualization with fluorophores Opal 520, Opal 540, Opal 570, Opal 620, Opal 650, and Opal 690 (Akoya

Biosciences) diluted in 1X Plus Amplification Diluent (Akoya Biosciences). Thus, in the seventh round, nuclei were counterstained with spectral DAPI (Akoya Biosciences) and the sections mounted with Faramount Aqueous Mounting Medium (Dako).

Respective immunostainings without primary antibodies were used as negative controls. At equal antibody concentrations, TSA-based visualization is expected to yield a greater number of positive cells compared with conventional immunofluorescence [14, 16]. We therefore established a singleplex TSA-based visualization of primary antibodies on control tonsil tissue and human lung TB granulomas as the gold standard for cell antigen visualization (Fig. 1e). Then, we performed a singleplex vs multiplex comparison for each antibody to validate the staining patterns in human tonsil and lung TB granulomas (Fig. 1c, e). Based on this comparison, we established the optimal signal through dilution of the primary antibodies and/or fluorophores to obtain staining levels and cell counts comparable to conventional immunofluorescence staining. The dilution of CD137 antibody was optimized to allow for the detection of membrane and cytoplasmic CD137 in a similar pattern to a previous description [17]. Using multiplex immunofluorescence to monitor false-positive results through incomplete antibody–TSA complex stripping and false-negative results through antigen masking (by incubation with multiple primary antibodies, umbrella-effect), single primary antibody staining was performed in parallel, and the results were then compared with those found using multiplex staining. Spillover effects were controlled for CD11b-, CD4-, and CD137-antibody staining of tonsil tissue with different Opal fluorophores by signal detection in adjacent cell components/channels and thereafter for exposure time settings upon acquisition of multiplex stained tissue sections.

Tissue imaging, spectral unmixing, and phenotyping

Multiplexed immunofluorescence slides were scanned on a Vectra Polaris Automated Quantitative Pathology Imaging System (Akoya Biosciences) as described earlier [13, 14, 16]. Briefly, a spectral library containing the spectral peaks emitted by each fluorophore from single stained slides was created using inForm software (version 2.4.8, Akoya Biosciences). This spectral library was used for spectral unmixing of the images, allowing color-based identification of the markers of interest. Autofluorescence was determined for unstained lung TB granuloma tissue used in this study cohort.

The entire granuloma present in a single FFPE tissue section, including the central area of necrosis and the surrounding cellular area at the periphery, was imaged using

Akoya Biosciences' Vectra Polaris imaging platform, resulting in several.im3 image tiles. Each image tile was spectrally unmixed and exported as a component TIF image tile using Akoya Biosciences' Inform software (version 2.4.8). Component TIF image tiles from each granuloma were then imported into the open source digital pathology software QuPath version 0.2.0-m9. The images were then stitched together using x–y coordinates to create a new pyramidal TIF file for image analysis (Supplementary Fig. 2). Image analysis was performed for the whole TB granuloma and referred to the total granuloma area (Supplementary Table 1).

Cell segmentation was performed for the whole granuloma multispectral image using QuPath software version 0.2.0-m9 [18]. Nuclear detection was carried out using the DAPI channel with a custom, unsupervised watershed algorithm. Cellular debris, usually found within the central necrotic areas, was not detected. Each detected nucleus was then expanded to provide an approximation of the full cell area, constrained by the distance and proximity of neighboring cells (Supplementary Figs. 3a, b and 4a, b). A list of several features derived from cell morphometry and intensity measurements was then calculated for each cell as previously described [18]. A random trees algorithm classifier was trained separately for each cell marker using the features generated earlier by having an experienced pathologist annotate regions in a subset of images (a training set) obtained from all lung TB granulomas used in this study, with interactive feedback on the classification performance provided during training in the form of a markup image, as described previously (Supplementary Figs. 3c–g and 4c–g) [18, 19]. Cells close to the border of the images were removed to reduce the risk of artifacts.

Based on the fluorescence panels, cells were further subclassified as CD11b+, CD68+, CD3+, CD8+, CD4+, CD3+, and CK+. For the myeloid and lymphoid cell panel, CD4+ T cells were defined as CD3+ CD8−. CK was used to visualize epithelial cells of the lung. For the reactive T-cell panel, subpopulations within CD4+ and CD8+ T cells were then classified by the presence and absence of three additional markers: FOXP3, PD-1, and CD137. The staining pattern for CD137 considered as positive has been described previously [17]. Cells negative for these markers were defined as "other cell types".

PD-L1 and CTLA-4 immunohistochemistry

The PD-L1 immunohistochemistry staining protocol using the PD-L1 IHC 22C3 pharmDx kit was performed as specified in the pharmDx kit label. Slides were processed on the Autostainer Link 48 (Agilent Technologies, Santa Clara, CA) alongside with control slides, using an automated staining protocol that had been validated for the PD-L1 immunohistochemistry assay, and prepared using EnVision FLEX Target Retrieval Solution, Low pH (Dako, Glostrup, Denmark). The 22C3 antibody was provided already diluted at an unspecified ratio.

CTLA-4 immunohistochemistry staining (clone BNI3, 1:50, product number: ab151773, Abcam, Cambridge, UK) was performed on a Roche Ventana BenchMark ULTRA Slide Stainer (Ventana Medical Systems, Inc. USA) platform with the OptiView DAB IHC detection kit. Normal placental sections served as positive tissue controls.

Statistics

Wilcoxon–Mann–Whitney tests were applied to identify immune markers that reached a significant difference in density levels among granulomas with positive and negative AFB staining for Mtb. For the correlation analyses between different lymphoid and myeloid cell marker distributions, the Spearman correlation coefficient (r) was calculated using RStudio 1.1.419 running R 3.4.3. All $r = 0$ values indicated no association between features; $r > 0$ indicated a positive association where as one variable increases, so does the other; and $r < 0$ indicated a negative association where as one variable increases, the other decreases. All $p < 0.05$ values were considered statistically significant.

Results

Multiplexed immunofluorescence assays development and validation

We established two multiplex immunolabeling protocols based on TSA using Opal fluorophores (Fig. 1a–e and Supplementary Fig. 1), which allowed for the simultaneous visualization and quantification of six cellular markers for each panel in a single FFPE tissue section. Multispectral imaging followed by spectral unmixing and digital pathology were applied to the six-marker-stained samples, allowing the simultaneous evaluation of all cell markers. A comparison of the unmixed seven-color multispectral image (six cellular markers plus DAPI) from multiplex stained tissues with tissue sections individually stained (singleplex) for each cell marker showed the efficacy of the spectral unmixing algorithm and demonstrated that the total cell counts were similar in both singleplex and multiplex assays (Fig. 1c, d).

As anticipated, TSA-based visualization detected a slightly greater number of positive cells. Although staining variation was observed between singleplex and multiplex, overall the markers had similar cell counts (Fig. 1c–e). Similar patterns of staining and distribution for each marker were observed with both immunofluorescence techniques. In addition, two replicates of full multiplex

immunofluorescence assays were performed on different days displaying similar results (Fig. 1b).

For the reactive T-cell multiplex panel, the CD4 marker showed a diffuse granular membrane staining with variable levels of background in the tissue. CD4 marker was also detected on cells that morphologically resembled macrophages. As previously reported by our group, in normal tonsil, the CD137 immunostaining pattern is characteristically seen within secondary lymphoid follicles. In tonsil, CD137 is expressed by lymphocytes on the cell surface as well as in the cytoplasm and Golgi apparatus [17]. A similar pattern of expression and distribution was observed using both immunofluorescence techniques (Supplementary Fig. 1).

As cell segmentation is based on the DAPI wavelength, accurate detection and segmentation of macrophage nuclei is not always possible. Macrophages are large cells, and often only parts of the cytoplasm and cell membrane can be observed in 4-μm sections.

Heterogeneous immune environment on TB granulomas

The demographics of the patients are shown in Supplementary Table 1. Histologically, TB granulomas were typically characterized by central necrosis and liquefaction caused by the immune activation occurring at this site [5]. This process is primarily mediated by monocytes, macrophages, and CD4+ and CD8+ T cells [20, 21].

To characterize the immune infiltrate, we used seven-color multiplex immunostaining (CD20, CD3, CD8, CD11b, CD68, CK, and DAPI) to estimate five different immune infiltrate subpopulations in large areas of TB granulomas from 14 different patients (Supplementary Table 1). The measured granuloma area is subject to the location of sectioning and may not accurately reflect the true size of the lesion. A total of ~463,868 cells were counted for both panels and evaluated by digital pathology (Supplementary Figs. 3 and 4). We observed diverse cellular compositions of the granuloma immune environments. There was a clear heterogeneous distribution of B and T lymphocytes in the different granulomas. The relative CD20, CD4, CD8, and CD11b frequency within each TB granuloma is shown in Fig. 2a–c and suggested that granulomas exhibited morphological heterogeneity. The immune infiltrate in TB lesions was predominately caused by the accumulation of CD20, CD4, and CD8-expressing cells. Relatively similar numbers of the myeloid cell marker CD11b was found in the different granulomas.

We next sought to identify whether specific immune cell infiltration was more predominately present in TB granulomas where AFB had been detected by light microscopy. AFB were identified in 9 of 14 TB granulomas (Supplementary Table 2). Significantly more cells expressing the phagocytic cell marker CD68 of macrophages and CD8+ T cells were found in granulomas that were AFB-positive (Supplementary Table 2). The immune densities of CD68+ macrophages and CD8+ T cells were greater in the presence of AFB compared with granulomas that were AFB-negative (p value = 0.007 and 0.012, respectively). The myeloid markers CD11b, CD3+, and CD4+ T cells and CD20+ B lymphocytes did not correlate with the presence of AFB as detected by Ziehl–Neelsen staining and light microscopy (Supplementary Table 2).

Immune cell densities on TB granulomas

Macrophages play crucial role in TB granuloma formation. Infected macrophages that are unable to control bacillary growth undergo caseous necrosis. Leukocytes are recruited to surround the zone of caseous necrosis to form a highly cellular area that contributes to limiting the spread of Mtb [22, 23].

The immune cell densities in the central necrotic zones and surrounding cellular areas at the periphery were characterized and quantified using panels of antibodies targeting the myeloid marker CD11b, the phagocytic cell marker CD68 of macrophages (CD68+), CD3+, and CD8+ T cells and CD20+ B lymphocytes (Fig. 3a–c). Consistent with our immune phenotyping findings, heterogeneity in immune cell densities of lymphoid and myeloid cell markers was observed in all granulomas (Fig. 3a–c). Numerous CD68+ macrophages and few T cells were observed in the necrotic areas, thereby possibly preventing direct T-cell–macrophage interactions. In an effort to determine the association between the immune cell densities of lymphoid and myeloid cell markers, we performed a Spearman correlation analysis. We found that CD8+ T-cell densities were individually strongly correlated with the myeloid cell markers CD11b and CD68 in a correlation analysis (Spearman's rank-order correlation; $r = 0.68$ for CD11b; 0.75 for CD68; $p < 0.01$), but only moderately correlated with CD3 (Spearman's rank-order correlation; $r = 0.42$ for CD11b; 0.49 for CD68; $p < 0.01$) (Fig. 3d). The myeloid cell markers CD11b and CD68 also seemed to be weakly associated with other lymphocyte markers in the correlation matrix.

FOXP3-expressing regulatory T cells and reactive T cells on TB granulomas

Cell-mediated immunity is critical for host defense against Mtb and is based on cellular interactions mediated by CD4+ and CD8+ T cells. FOXP3-expressing regulatory T cells are a subset of CD4+ T cells and have recently been shown to suppress antimicrobial immune responses [24]. The percentage of CD4+ and CD8+ T cells expressing FOXP3 was further investigated in nine TB granulomas using an additional fluorescence multiplex panel containing the markers CD8, CD4, and FOXP3 (Fig. 4a). FOXP3
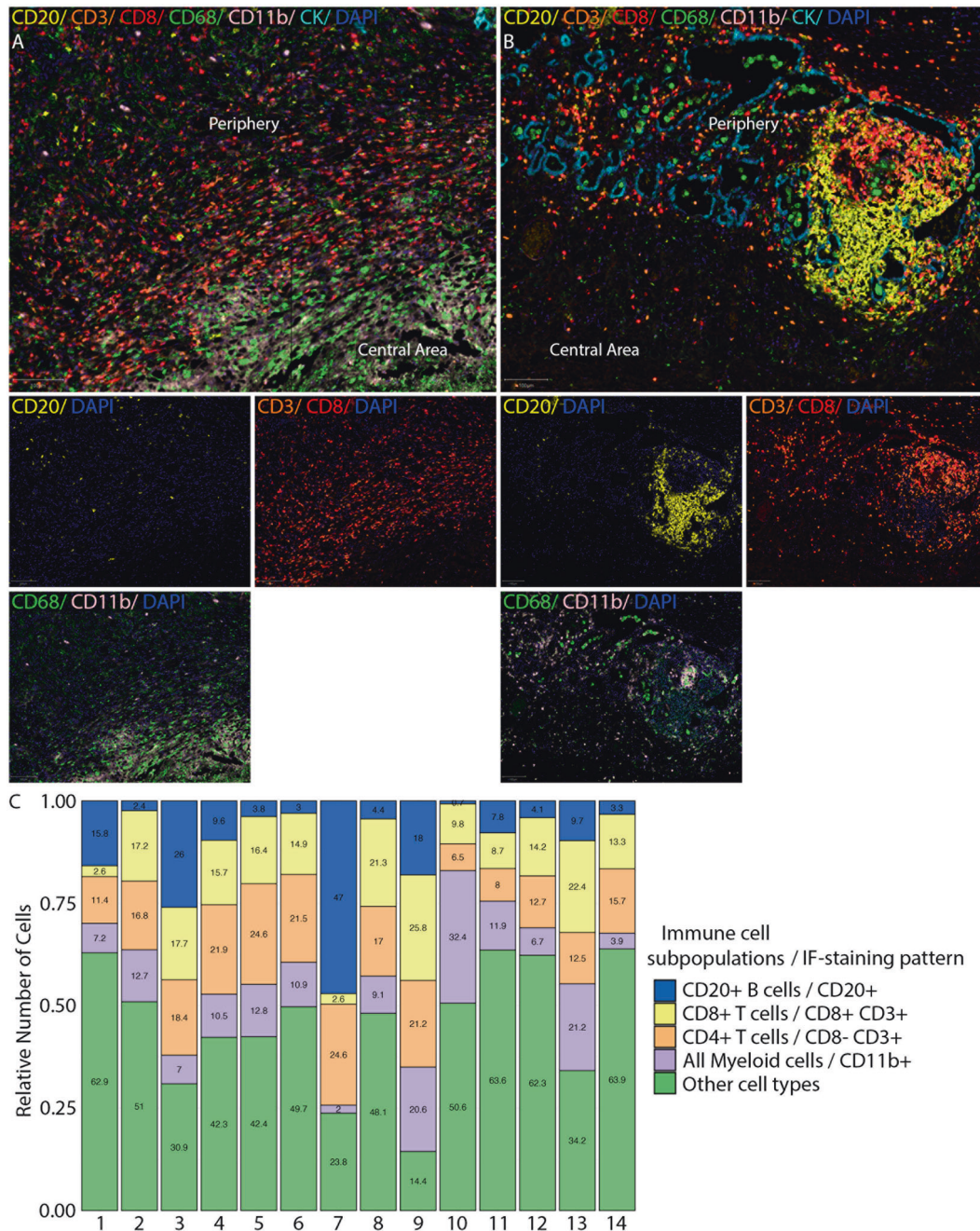
Fig. 2 Immune environments on TB granulomas. a TB granuloma enriched for T cells and myeloid phenotypes with minimal B cell infiltration. **b** TB granuloma enriched for T and B cell phenotypes. **a**, **b** Full composite image and images for each individual marker and different combinations from the composite image are shown. **c** Relative frequency of different immune phenotypes of the nine TB granulomas and marker combinations used to identify immune subpopulations by seven-color multiplex immunostaining. Central and periphery areas of lung TB granulomas are shown. Scale bars represent 100 μm.

expression was limited to a small subset of CD4+ T cells. CD4+FOXP3+ cells represented 0.1–3.4% of the total CD4+ T cells (Fig. 4b).

CD4+ and CD8+ T cells reactive to TB antigens and epitopes are associated with an extensive diversity of immunodominant responses in infected individuals. In an attempt to identify the reactive T-cell fraction in nine TB granulomas, we used a multiplexed analysis to simultaneously measure CD4+ and CD8+ T cells and the expression of the T-cell activation markers CD137 and PD-1 (Fig. 5a, b). A small fraction of total CD4+ and CD8+

Fig. 3 Immune cell densities on TB granulomas. a TB granuloma with relatively low expression of the myeloid cell markers CD11b and CD68, CD3+ and CD8+ T cells and CD20+ B lymphocytes. **b** TB granuloma enriched for myeloid, T and B cell phenotypes. **a**, **b** Full composite image and images for each individual marker are shown. Central and peripheral areas of lung TB granulomas are shown. **c** Cell densities (cell/mm^2) of different immune phenotypes of nine TB granulomas and marker combinations used to identify immune subpopulations by seven-color multiplex immunostaining. **d** Spearman correlation matrix for lymphocyte densities (CD20, CD3, CD4, CD8) and myeloid densities (CD11b, CD68). The Spearman correlation coefficient is shown for all relationships. A coefficient with a value of either +1 (blue), 0 (white), or −1 (red) indicates a perfect association, no association, and a perfect negative association of ranks, respectively. Numbers indicate the correlation coefficient. Correlations with a *p* value > 0.01 were considered insignificant, as indicated by crosses. Scale bars represent 100 µm.
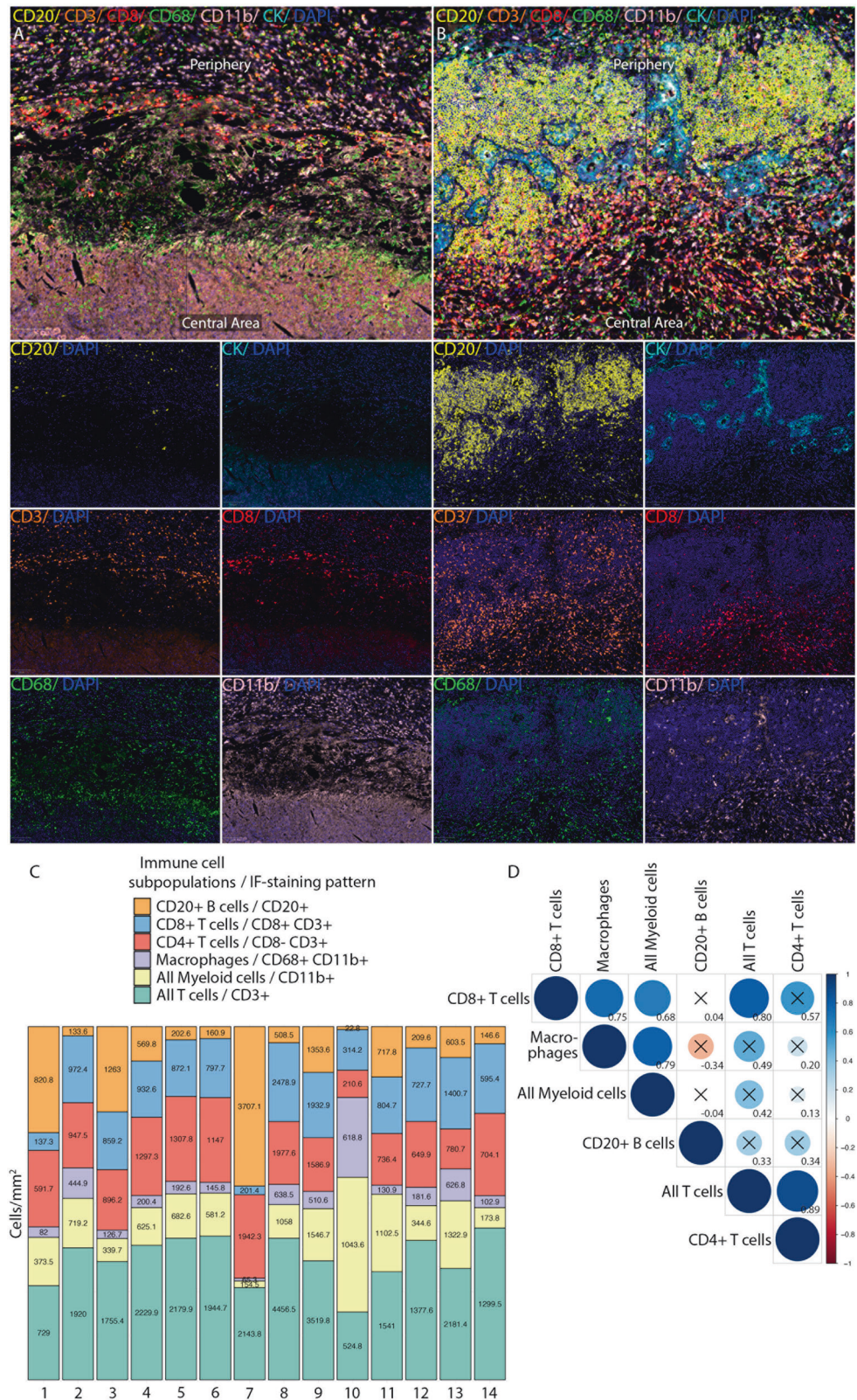
T cells expressed PD-1, representing 0–3% of the total CD4+ T cells and 0–1.8 of the total CD8+ T cells (Fig. 5c). CD137 expression on T cells was detected in a very small fraction of CD4+ T cells in two granulomas, representing only 0.1 and 0.2% of the total CD4+ T cells (Fig. 5c).
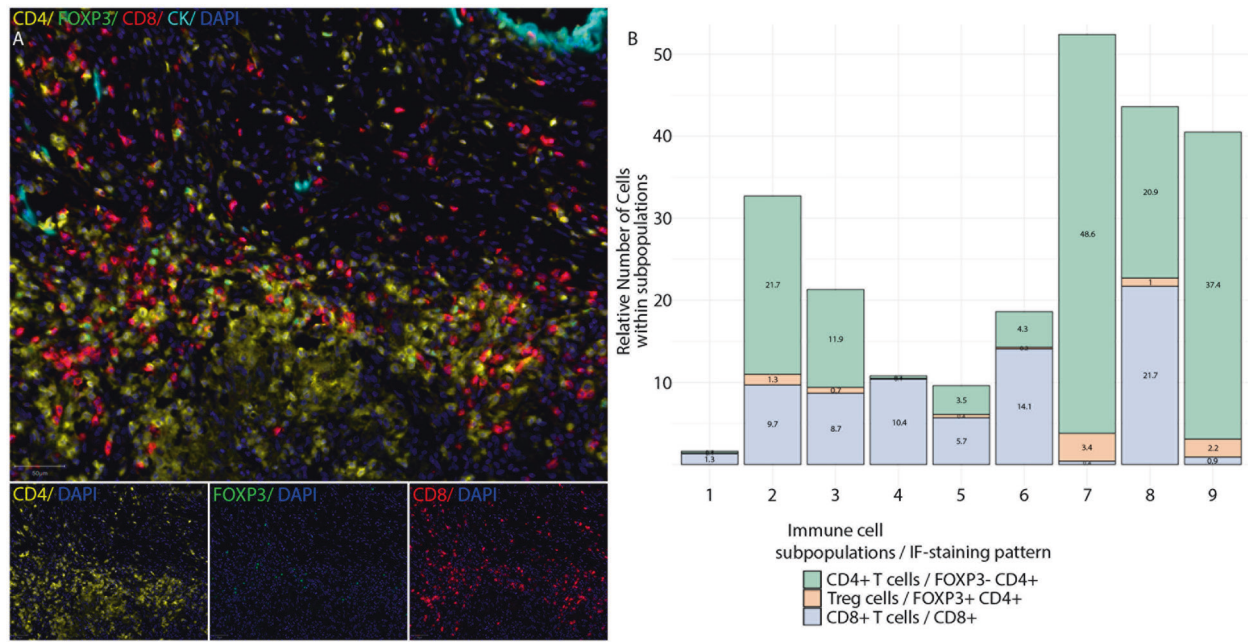
Fig. 4 FOXP3-expressing regulatory T cells on TB granulomas. a Confirmation of FOXP3 expression in CD4+ T cells by double marker immunostaining and images for each individual marker are shown.

b Relative number of cells expressing FOXP3 among CD4+ and CD8+ T cells and marker combinations used to identify immune subpopulations by multiplex immunostaining. Scale bars represent 50 μm.

PD-L1 and CTLA-4 expression on multinucleated giant cells

Macrophages, which later differentiate into MGCs, are recruited to the site of Mtb infection. These cells displayed moderate to strong membrane PD-L1 staining (Fig. 6a–c). Weak cytoplasmatic PD-L1 staining was also observed. Although the internal positive control (lymphocytes) was positive, no immunoreaction was detected on epithelioid macrophages and MGCs with CTLA-4 antibody (Fig. 6d–f).

Discussion

The precise nature of the local immune responses in lung TB granulomas requires a comprehensive understanding of their environmental complexities [25, 26]. The use of multiple cellular markers is essential because it allows for the identification of different cell subpopulations in one tissue section [12–14]. Multiplexed analysis can also simultaneously measure the expression of distinct markers in a single cell and the spatial associations between immune cell subpopulations. Here, we established two complementary multiplex immunolabeling panels to simultaneously assess six markers in a single FFPE tissue section for each panel. We applied this technology to evaluate the complex immune environment of a small series of confirmed cases of lung TB granulomas.

At its most basic level, a granuloma is a compact, organized immune aggregate of macrophages that arises at the site of Mtb infection [2]. Macrophages later differentiate into specialized cell types, including epithelioid macrophages and MGCs. Many other cell types also populate the granuloma, including myeloid cells, B and T cells that surround the macrophage-rich center [2, 27]. Over time, some granulomas can undergo complex remodeling events that are characterized by central necrosis (caseum), formed by the death of participating cells [28]. The multiplex cellular analyses provided us an opportunity to demonstrate that human lung TB granulomas contain a heterogeneous immune environment. We showed a variance between different CD3+ and CD8+ T cells and CD20+ B lymphocyte subpopulations of different granulomas. This result suggested diverse lymphocyte compositions of the granuloma immune environments, with the density of CD8+ T-cell potentially being influenced by the presence of MTb. We also observed a relatively homogeneous distribution of the myeloid cell marker CD11b, which was used to evaluate the innate immune composition of TB granulomas.

The diverse CD3+ and CD8+ T-cell and CD20+ B lymphocyte distribution suggested that some TB granulomas were immunologically reactive, with more immune cell recruitment and/or replication than others, representing distinct immune environments. Our data suggest that the distribution and relative abundance of cells expressing the phagocytic cell marker CD68 of macrophages and CD8+ T cells may be influenced by the presence of Mtb. This
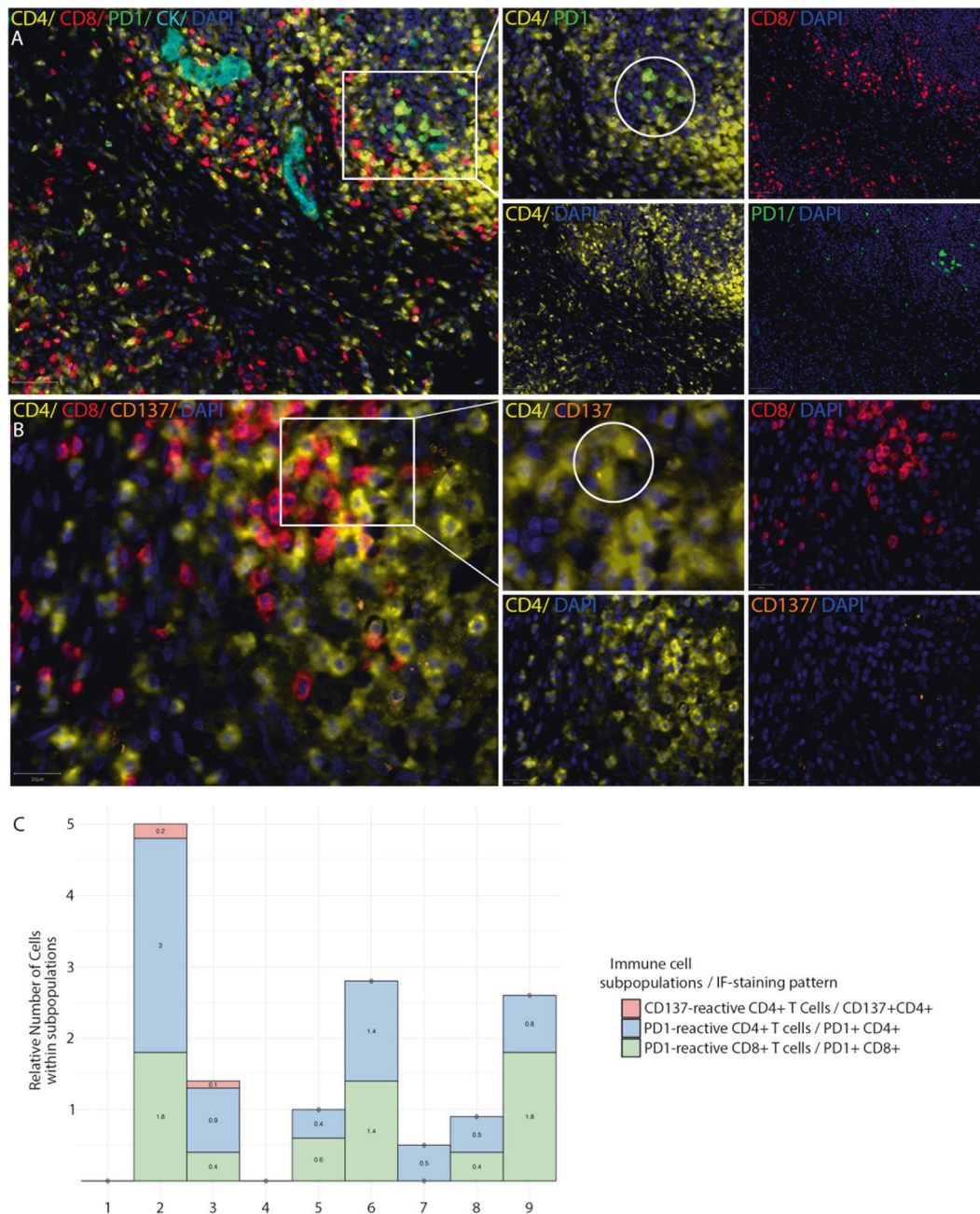
Fig. 5 Reactive CD4+ and CD8+ T cells on human lung TB granulomas. a Confirmation of PD-1 expression in CD4+ or CD8+ T-cell subpopulations by double marker immunostaining and images for each individual marker are shown. One field from the full composite image with a circle depicting several PD-1-reactive CD4+ T cells. **b** Confirmation of CD137 expression in CD4+ T cells by double marker immunostaining and images for each individual marker are shown. One field from the full composite image with a circle depicting two CD137-reactive CD4+ T cells from the full composite image. **c** Relative number of reactive T cells within CD4+ and CD8+ T-cell subpopulations and marker combinations used to identify immune subpopulations by multiplex immunostaining. CD137 (4-1BB) and PD-1 were used as markers for reactive T cells. Scale bars represent the following: **a**, 20 μm; **b**, 50 μm.

result is in accordance with the idea that the immune microenvironments in TB granulomas might be determined, at least in part, by the local leukocyte response to the bacillary load. Recent observations have suggested that the structural, microbiological, and immunological hetero-geneity of TB granulomas might be mediated by the quality of the local immune response and the level of inflammation [26]. Thus, the various immunologic factors influencing the quality of local lung responses might determine the varied outcomes of infection [25]. Our results suggested that the detection of granulomas positive for AFB in association with the number of infiltrating CD8+ T cells and
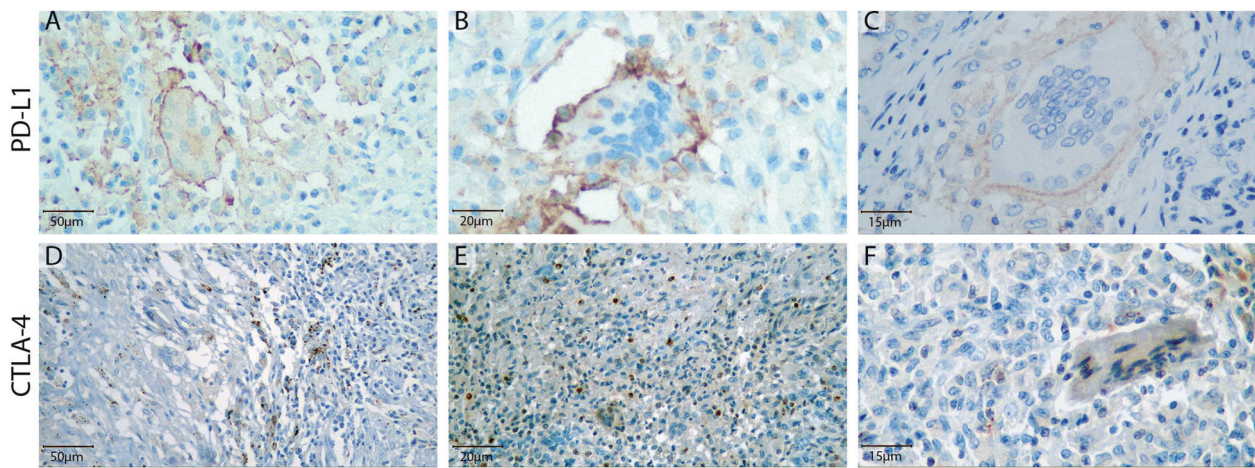
Fig. 6 PD-L1 and CTLA-4 expression on differentiated macrophages. Multinucleated giant cells showing strong PD-L1 membrane staining (**a–c**) and no CTLA-4 staining (**d–f**) in three different lung granulomas. The internal positive control (lymphocytes) was strongly positive. Scale bars represent the following: **a** and **d**, 50 μm; **b** and **e**, 20 μm; **c** and **f**, 15 μm.

macrophages may be a determinant of TB granuloma immunogenicity. One limitation of our study is the small number of lung TB granuloma sections examined. In addition, for image analysis, we evaluated the whole TB granuloma area instead applying the region-based approach, which divides the granulomas into two areas: (1) zone of caseous necrosis and (2) surrounding highly cellular area. The development of image analysis algorithms that reliably segment granulomas into these two areas is challenging. The whole granuloma analysis approach might not accurately reflect the true size of the lesion and might have precluded the ability to address complex issues involving the immune environmental composition of TB granulomas.

Adaptive immune responses, including CD8+ T-cell activity, are required to eradicate infection. Macrophages are the key targets of Mtb infection. CD8+ T cells use granule-dependent killing to eliminate infected target cells at the site of infection [29]. The exploration of the immune environmental composition of TB granulomas in one tissue section revealed significant associations between CD8+ T-cell densities and the myeloid marker CD11b and phagocytic cell marker CD68. In addition, an association between CD3+ T-cell and the myeloid cell markers CD11b and CD68 was also found. T cells are continuously recruited to nonsterile granulomas, while sterile granulomas are maintained with the minimum required cell numbers for continued maintenance [30]. Mtb infection induces CD8+ T cells. CD8+ T cells are able to recognize Mtb-specific antigens (as peptides) presented by classical and non-classical MHC molecules [5]. Our results also suggest that the distribution of cytotoxic CD8+ T cells may be particularly significant when found in the direct vicinity of the central necrotic areas of nonsterile granulomas.

CD4+ T cells also play an import role in host immune responses to Mtb infection. A deficiency of CD4+ T cells in

humans, particularly those who are HIV+, dramatically increases susceptibility to both primary or reactivation TB [31]. To be effective, CD4+ and CD8+ T cells must be activated by interactions with infected macrophages. Activated T cells release cytokines to activate the antimicrobial capacity of macrophages or kill the cell via cytotoxic mechanisms [5]. The granuloma structure may prevent T-cell-infected macrophage interactions. The macrophage-rich center, which is often necrotic, may prevent interactions with surrounding T cells [5]. Another limitation of our study is that the bacterial burden was not available.

During TB, FOXP3 expression is restricted primarily to CD4+ T cells [32]. FOXP3-expressing regulatory T (T reg) cells are a subset of CD4+ T cells that may be needed to prevent excessive immunopathology in tissue. We further demonstrated that FOXP3 expression was predominately found in a small subset of CD4+ T cells. T reg infiltration levels varied, but they still represented a small subpopulation of the T lymphocytic landscape in lung granulomas. The recruitment of T reg cells at primary sites of Mtb infection might lead to their capacity to influence the ability of CD8+ T cells to promote protective immune responses [32].

The success or failure of each granuloma is determined by the immune response within that granuloma at a local but not a systemic level [30]. Despite the inflammation in TB lesions, the levels of perforin or granulysin are relatively low [5]. In animal models, only limited numbers of T cells produce cytokines at the site of disease, which nonetheless is still able to control bacterial burden [30].

In oncology, the principle that naturally occurring T cells with anti-tumor potential exist in human cancer has rationalized the application of immunotherapy [33]. CD137, also called 4-1BB, is a member of the TNF receptor superfamily with T-cell costimulatory functions [34]. Signaling through

CD137 by its natural ligand, CD137L enhances T-cell cytolytic effector functions. Naïve T cells do not express CD137; upon stimulation, activated T cells transiently express high levels of CD137, which disappears rapidly [33]. CD137 expression has been used to identify reactive T cells in response to antigen without knowledge of the epitope specificities [35]. Thus, the expression of CD137 on T cells is tightly regulated and extremely sensitive in response to antigen stimulation. PD-1 has also been reported to be used as a biomarker to identify reactive T cells [36]. PD-1 is a negative immunoregulatory molecule that is expressed by activated T cells and plays an important role in the immunobiology of cancer [37].

To identify reactive T cells in lung TB granulomas, we used a multiplex analysis to simultaneously detect the expression of CD137 and PD-1 on T cells. We showed that only a small fraction of the CD4+ and CD8+ T cells expressed PD-1. CD137 expression was only found on a very small fraction of the CD4+ T cells in two granulomas. PD-1 expression is associated with T-cell exhaustion following constant exposure to antigen [37, 38]. In animal models, PD-1+ T cells are rarely seen in TB granulomas [30]. Thus, T-cell exhaustion does not appear to account for the low frequencies of cytokine-producing T cells in TB granulomas [30].

T-cell–macrophage interactions are modulated by several signals provided by costimulatory molecules, including CTLA-4 and PD-1. PD-1 inhibits T-cell activation when it binds to its ligands PD-1 ligand-1 (PD-L1, also called B7-H1). Our results showed that MGCs exhibited strong PD-L1 membrane staining, but not CTLA-4. This result suggested that the adaptive immune response could play a role in preventing granuloma progression. In animal models, surprisingly and paradoxically, PD-1-deficient mice present extreme sensitivity to Mtb, showing massive bacterial proliferation in the lung [39]. This phenomenon raises the issue of whether the PD-1/PD-L1 pathway might also have a role in regulating early innate and inflammatory responses after infection. In addition, PD-1$^{-/-}$ mice showed a substantially increased inflammatory and necrotic response to Mtb in the absence of PD-1, indicating an essential role for this coinhibitory receptor in controlling inflammatory responses to a highly immunogenic pathogen [39]. In human TB pleural effusion samples, blockade of the PD-1/PDL-1 signaling pathway enhances cytotoxic degranulation of CD8+ T cells [40]. In addition, PD-L1 blockade has been shown to increase macrophage susceptibility to death by enhancing the cytotoxic potential of CD8+ T cells [41]. Additional research is needed to help to guide development of potential novel immunotherapy strategies for TB.

This study offers new insights into the heterogeneity of immune cell infiltration in TB granulomas, suggesting that each TB granuloma represents a unique immune environment that might be independently influenced by the local adaptive immune response, bacterial state, and overall host disease status.

Compliance with ethical standards

References

1. Pai M, Behr MA, Dowdy D, Dheda K, Divangahi M, Boehme CC. et al. Tuberculosis. Nat Rev Dis Prim. 2016;2:16076.
2. Ramakrishnan L. Revisiting the role of the granuloma in tuberculosis. Nat Rev Immunol. 2012;12:352–66.
3. World Health Organization (WHO), Global tuberculosis report 2019, Geneva, 2019. Licence: CCBY-NC-SA3.0IGO.
4. Hunter RL. The pathogenesis of tuberculosis: the early infiltrate of post-primary (adult pulmonary) tuberculosis: a distinct disease entity. Front Immunol. 2018;9:2108.
5. Lin PL, Flynn JL. CD8 T cells and Mycobacterium tuberculosis infection. Semin Immunopathol. 2015;37:239–49.
6. Lay G, Poquet Y, Salek-Peyron P, et al. Langhans giant cells from M. tuberculosis-induced human granulomas cannot mediate mycobacterial uptake. J Pathol. 2007;211:76–85.
7. van Rie A, Warren R, Richardson M, Victor TC, Gie RP, Enarson DA, et al. Exogenous reinfection as a cause of recurrent tuberculosis after curative treatment. N Engl J Med. 1999;341:1174–9.
8. Saunders BM, Britton WJ. Life and death in the granuloma: immunopathology of tuberculosis. Immunol Cell Biol. 2007;85:103–11.
9. Andersson J, Samarina A, Fink J, Rahman S, Grundström S. Impaired expression of perforin and granulysin in CD8+ T cells at the site of infection in human chronic pulmonary tuberculosis. Infect Immun. 2007;75:5210–22.
10. Ulrichs T, Lefmann M, Reich M, Morawietz L, Roth A, Brinkmann V, et al. Modified immunohistological staining allows detection of Ziehl-Neelsen-negative *Mycobacterium tuberculosis* organisms and their precise localization in human tissue. J Pathol. 2005;205:633–40.
11. Somoskovi A, Dormandy J, Rivenburg J, Pedrosa M, McBride M, Salfinger M. Direct comparison of the GenoType MTBC and genomic deletion assays in terms of ability to distinguish between members of the Mycobacterium tuberculosis complex in clinical isolates and in clinical specimens. J Clin Microbiol. 2008;46:1854–7.

12. Martinez-Valbuena I, Valenti-Azcarate R, Amat-Villegas I, Riverol M, Marcilla I, de Andrea CE, et al. Amylin as a potential link between type 2 diabetes and alzheimer disease. Ann Neurol. 2019;86:539–51.

13. Gorris MAJ, Halilovic A, Rabold K, van Duffelen A, Wickramasinghe IN, Verweij D, et al. Eight-color multiplex immunohistochemistry for simultaneous detection of multiple immune checkpoint molecules within the tumor microenvironment. J Immunol. 2018;200:347–54.

14. Parra ER, Uraoka N, Jiang M, Cook P, Gibbons D, Forget MA, et al. Validation of multiplex immunofluorescence panels using multispectral microscopy for immune-profiling of formalin-fixed and paraffin-embedded human tumor tissues. Sci Rep. 2017;7: 13380.

15. Schalper KA, Rodriguez-Ruiz ME, Diez-Valle R, López-Janeiro A, Porciuncula A, Idoate MA, et al. Neoadjuvant nivolumab modifies the tumor immune microenvironment in resectable glioblastoma. Nat Med. 2019;25:470–6.

16. Griss J, Bauer W, Wagner C, Simon M, Chen M, Grabmeier-Pfistershammer K, et al. B cells sustain inflammation and predict response to immune checkpoint blockade in human melanoma. Nat Commun. 2019;10:4186.

17. Alfaro C, Echeveste JI, Rodriguez-Ruiz ME, Solorzano JL, Perez-Gracia JL, Idoate MA, et al. Functional expression of CD137 (4-1BB) on T helper follicular cells. Oncoimmunology. 2015;4: e1054597.

18. Bankhead P, Fernández JA, McArt DG, Boyle DP, Li G, Loughrey MB, et al. Integrated tumor identification and automated scoring minimizes pathologist involvement and provides new insights to key biomarkers in breast cancer. Lab Invest. 2018;98:15–26.

19. Breiman L. Random forests. Mach Learn. 2001;45:5–32.

20. Grotzke JE, Lewinsohn DM. Role of CD8+ T lymphocytes in control of Mycobacterium tuberculosis infection. Microbes Infect. 2005;7:776–88.

21. Boer MC, Joosten SA, Ottenhoff THM. Regulatory T-Cells at the interface between human host and pathogens in infectious diseases and vaccination. Front Immunol. 2015;6:217.

22. Subbian S, Tsenova L, Kim MJ, Wainwright HC, Visser A, Bandyopadhyay N, et al. Lesion-Specific immune response in granulomas of patients with pulmonary tuberculosis: a pilot study. PLoS ONE. 2015;10:e0132249.

23. Reece ST, Kaufmann SHE. Floating between the poles of pathology and protection: can we pin down the granuloma in tuberculosis? Curr Opin Microbiol. 2012;15:63–70.

24. Cardona P, Cardona P-J. Regulatory T Cells in Mycobacterium tuberculosis infection. Front Immunol. 2019;10:2139.

25. Cadena AM, Fortune SM, Flynn JL. Heterogeneity in tuberculosis. Nat Rev Immunol. 2017;17:691–702.

26. Carow B, Hauling T, Qian X, Kramnik I, Nilsson M, Rottenberg ME. Spatial and temporal localization of immune transcripts defines hallmarks and diversity in the tuberculosis granuloma. Nat Commun. 2019;10:1823.

27. Pagán AJ, Ramakrishnan L. Immunity and immunopathology in the tuberculous granuloma. Cold Spring Harb Perspect Med. 2015;5:a018499.

28. Ndlovu H, Marakalala MJ. Granulomas and inflammation: host-directed therapies for tuberculosis. Front Immunol. 2016;7:434.

29. Rahman S, Gudetta B, Fink J, Granath A, Ashenafi S, Aseffa A, et al. Compartmentalization of immune responses in human tuberculosis. Am J Pathol. 2009;174:2211–24.

30. Gideon HP, Phuah J, Myers AJ, Bryson BD, Rodgers MA, Coleman MT, et al. Variability in tuberculosis granuloma T cell responses exists, but a balance of pro- and anti-inflammatory cytokines is associated with sterilization. PLoS Pathog. 2015;11: e1004603.

31. Serbina NV, Lazarevic V, Flynn JL. CD4+ T Cells are required for the development of cytotoxic CD8+ T cells during Mycobacterium tuberculosis infection. J Immunol. 2001; 167:6991–7000.

32. Scott-Browne JP, Shafiani S, Tucker-Heard G, Ishida-Tsubota K, Fontenot JD, Rudensky AY, et al. Expansion and function of Foxp3-expressing T regulatory cells during tuberculosis. J Exp Med. 2007;204:2159–69.

33. Ye Q, Song DG, Poussin M, Yamamoto T, Best A, Li C, et al. CD137 accurately identifies and enriches for naturally occurring tumor-reactive T cells in tumor. Clin Cancer Res. 2014;20:44–55.

34. Zhu Y, Chen L. CD137 as a biomarker for tumor-reactive t cells: finding gold in the desert. Clin Cancer Res. 2014;20:3–5.

35. Wolfl M, Kuball J, Ho WY, Nguyen H, Manley TJ, Bleakley M, et al. Activation-induced expression of CD137 permits detection, isolation, and expansion of the full repertoire of CD8+ T cells responding to antigen without requiring knowledge of epitope specificities. Blood. 2007;110:201–10.

36. Inozume T, Hanada K, Wang QJ, Ahmadzadeh M, Wunderlich JR, Rosenberg SA, et al. Selection of CD8+PD-1+ lymphocytes in fresh human melanomas enriches for tumor-reactive T cells. J Immunother. 2010;33:956–64.

37. Topalian SL, Hodi FS, Brahmer JR, Gettinger SN, Smith DC, McDermott DF, et al. Safety, activity, and immune correlates of anti–PD-1 antibody in cancer. N Engl J Med. 2012;366:2443–54.

38. Pardoll DM. The blockade of immune checkpoints in cancer immunotherapy. Nat Rev Cancer. 2012;12:252–64.

39. Lázár-Molnár E, Chen B, Sweeney KA, Wang EJ, Liu W, Lin J, et al. Programmed death-1 (PD-1)-deficient mice are extraordinarily sensitive to tuberculosis. Proc Natl Acad Sci USA. 2010;107:13402–7.

40. Jurado JO, Alvarez IB, Pasquinelli V, Martínez GJ, Quiroga MF, Abbate E, et al. Programmed death (PD)-1:PD-ligand 1/PD-ligand 2 pathway inhibits T cell effector functions during human tuberculosis. J Immunol. 2008;181:116–25.

41. Suarez GV, Melucci Ganzarain CDC, Vecchione MB, Trifone CA, Marín Franco JL, Genoula M, et al. PD-1/PD-L1 pathway modulates macrophage susceptibility to Mycobacterium tuberculosis specific CD8+ T cell induced death. Sci Rep. 2019;9:187.